Available online at www.sciencedirect.com

ScienceDirect

journal homepage: www.elsevier.com/locate/he

Assessment of ammonia as energy carrier in the use with reversible solid oxide cells

Michele Zendrini [a,*], *Matteo Testi* [a], *Martina Trini* [a], *Penchini Daniele* [b], *Jan Van Herle* [c], *Luigi Crema* [a]

[a] *Fondazione Bruno Kessler, Via Sommarive 18, 38123, Trento, TN, Italy*
[b] *SOLIDPower Spa, Via Treno, 115/117, 38017, Mezzolombardo, TN, Italy*
[c] *EPFL SCI-STI-JVH, Rue de l'Industrie 17, Case Postale 440, CH-1951, Sion, Switzerland*

HIGHLIGHTS

- Ammonia efficiently feeds solid oxide fuel cells for combined generation.
- Higher efficiencies are obtained with ammonia rather than with hydrogen.
- Area-specific resistance for ammonia is larger than for hydrogen.

GRAPHICAL ABSTRACT

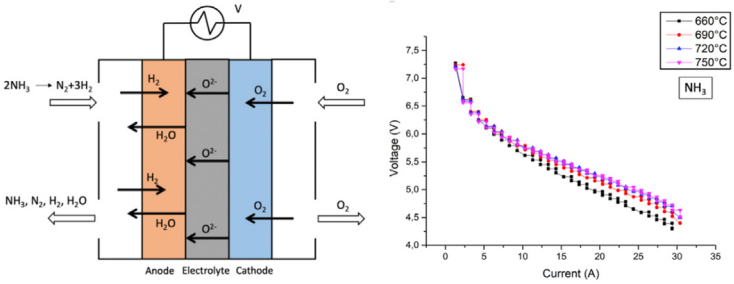

ARTICLE INFO

Article history:
Received 12 April 2021
Received in revised form
14 June 2021
Accepted 17 June 2021
Available online 9 July 2021

Keywords:
Hydrogen
Ammonia
SOFC
Energy carrier
ASR

ABSTRACT

Ammonia represents one of the most promising potential solutions as energy vector and hydrogen carrier, having a higher potential to transport energy than hydrogen itself in a pressurized form. Furthermore, solid oxide fuel cells (SOFCs) can directly be fed with ammonia, thus allowing for immediate electrical power and heat generation. This paper deals with the analysis of the dynamic behavior of commercial SOFCs when fueled with ammonia. Several measurements at different temperatures have been performed and performances are compared with hydrogen and a stoichiometrically equivalent mixture of H_2 and N_2 (3:1 M ratio). Higher temperature led to smaller drops in voltage for both fuels, thus providing higher efficiencies. Ammonia resulted slightly more performant (48% at 760 °C) than hydrogen (45% at 760 °C), in short stack tests. Moreover, different ammonia-to-air ratios have been investigated and the stack area-specific resistance has been studied in detail by comparing numerical modeling predictions and experimental values.

Abbreviations: ASR, area-specific resistance; BCGO, gadolinium-doped barium cerate; BCNO, nitrogen-doped barium cerate; BCZY, yttria/zirconia-doped barium cerate; BSCF, $Ba_{1-x}Sr_xCo_{1-y}Fe_yO_3$; DA-SOFCs, direct-ammonia solid oxide fuel cells; LSC, $La_{1-x}Sr_xCoO_3$; LSM, $La_{1-x}Sr_xMnO_3$; LHV, lower heating value; OCV, open circuit voltage; SDC, samarium-doped ceria; SSAS, solid-state ammonia synthesis; SSC, $Sm_{1-x}Sr_xCoO_3$; YSZ, yttrium-stabilized zirconia.

* *Corresponding author.*
E-mail address: michelezendrini@gmail.com (M. Zendrini).

https://doi.org/10.1016/j.ijhydene.2021.06.139

Introduction

The need for transforming the global energy system is pushing researchers to investigate new, clean conversion technologies to mitigate climate change and meet the targets of the Paris agreement signed in April 2016. The trend towards decarbonization and renewable energy sources' integration should continue, considering that electricity consumption will further increase by up to 40% until 2050 [1–4].

In this framework, most of the decarbonization potential will come from Renewables, variable and intermittent by nature. The potential of energy vectors lies in providing a solution for the Renewables variability, mainly wind and solar. Hydrogen (H_2) for fuel cells is potentially a zero-emission solution to help leveling out the mismatch between energy demand and supply. Surplus energy coming from renewable sources can be stored in large quantities into chemical energy with the aim of reinjecting it for end-use when needed. Today hydrogen production is still predominantly fossil-fuel based, obtained by steam-methane or oil reforming, and coal gasification, thus avoiding carbon dioxide emissions only if appropriate carbon capture and storage are undertaken [5,6].

The need for sustainable long-term energy storage raises interest towards other chemicals than hydrogen, such as carbon-neutral hydrogen derivatives. Among these, ammonia (NH_3) can be considered as one of the most attractive energy vectors for both mobile and stationary applications. Like for hydrogen, it can be produced both from fossil fuels with the well-established Haber-Bosch process, or from renewable sources by providing electricity to electrolytic cells. The interest in ammonia comes from several advantages with respect to hydrogen. First, the energy density of NH_3 (18.85 MJ/kg) is comparable to that of fossil fuels, ranging from 20 MJ/kg for low-ranked coals to 50 MJ/kg for natural gas. Hydrogen is energy dense per mass (120 MJ/kg) but suffers from a volumetric disadvantage that imposes very high-pressure storage tanks (hundreds of bars) or very low temperature for liquefaction (close to 20 K at atmospheric pressure). Contrarily, ammonia, that contains 17.6% in weight of hydrogen, can be easily liquefied at ambient temperature by compressing at 0.8 MPa, thus avoiding issues in terms of physical safety [7–13].

Ammonia can be found in nature almost uniquely as ammonium salts and its original formation dates back to volcanic activity or comes from the decomposition of nitrogen-containing organic materials [14–16]. However, the annual demand of ammonia is far from being supplied by natural processes and NH_3 remains one of the most produced chemicals worldwide [17]. The leading pathway for ammonia production is the Haber-Bosch process which catalytically converts molecular nitrogen and hydrogen into ammonia according to the reaction in Eq. (1):

$$N_2 + 3H_2 \longrightarrow 2NH_3 \qquad \text{Equation 1}$$

Ammonia is currently produced and distributed at >200 million tons per year, mainly used for fertilizers [8]. The remaining portion (close to 20% of the whole production, depending on the specific year) is industrially utilized for several applications ranging from plastics' production to chemicals' synthesis [7,18–20].

In this regard, handling, storage, transportation and distribution are far easier both in terms of cost-effectiveness and regulations with respect to hydrogen. Indeed, two well-established technologies for liquid storage of ammonia are largely widespread. When dealing with large storage volumes, atmospheric pressure vessels up to 50000t can be utilized while for small quantities of ammonia (up to 1500t) the pressure storage at ambient temperature is generally preferred for economic savings [18]. Furthermore, reliable and efficient infrastructures for storage, transportation and distribution are already established in terms of pipelines, rails, shipments and others [7].

In the abovementioned conditions, handling ammonia would be several times cheaper than hydrogen when considering the same energy content. Storage of ammonia over half a year would cost almost 0.54 \$/kg-H_2 while the cost raises to 14.95 \$/kg-H_2 when dealing with pure hydrogen [7,21]. The reason why this is the case lies in the fact that ammonia has a much larger volumetric density than hydrogen as shown in Table 1 [22,23].

Regarding the possibility of exploiting ammonia as fuel, solid oxide fuel cells (SOFCs) result particularly interesting thanks to their fuel flexibility allowed by high operating temperature [22–38]. Additionally, these cells possess the attractive advantage of not emitting dangerous or harmful by-products. The schematic working principle of an oxygen ion conducting SOFC is shown in Fig. 1. Ammonia can be exploited as fuel in SOFCs since it can be preliminary cracked into its primary constituents (molecular nitrogen and hydrogen) or even directly fed into the cell. This last possibility refers to the so-called Direct-Ammonia Solid Oxide Fuel Cell (DA-SOFC) which do not require any external unit for fuel pre-treatment [39–43]. The possibility of directly injecting ammonia in SOFCs has been firstly investigated by *Wojcik* et al. in 2003 [44]. The equilibrium ammonia molar fraction in the gas phase reduces when temperature increases because of ammonia decomposition [25]. When temperature is raised above 550–600 °C, NH_3 is almost completely thermally cracked (99.95%) into nitrogen (N_2) and hydrogen (H_2) regardless of the pressure level [45,46].

Even if ammonia significantly decomposes already above 400 °C when only considering thermodynamic equilibrium, the kinetics of the process are too slow for practical applications [47]. Due to this sluggishness, the temperature needs to

Table 1 – Physical properties of ammonia, liquid hydrogen and gaseous hydrogen.

	Ammonia NH_3	Liquid hydrogen $H_{2,l}$	Gaseous hydrogen $H_{2,g}$
Density	610.33 kg/m^3	70.99 kg/m^3	17.86 kg/m^3 (@250 bar,20 °C)
Volumetric density	11.38 GJ/m^3	8.49 GJ/m^3	2.15 GJ/m^3
LHV	18.85 MJ/kg	120 MJ/kg	120 MJ/kg
Energy density	11.5 MJ/L	8.491 MJ/L	4.5 MJ/L (@690 bar,15 °C)

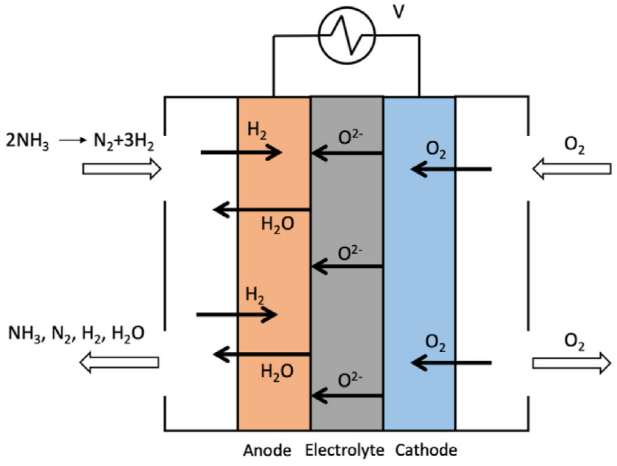

Fig. 1 – Schematic design and principle of operation of high temperature oxygen ion conducting solid oxide fuel cell.

be considerably raised or efficient catalysts need to be exploited. In the first investigations, Ag- and Pt-based electrodes with iron catalyst in a tubular oxygen ion conducting SOFC had been considered [44]. Successively, several studies have revealed that Ni possesses appreciable catalytic activity towards ammonia decomposition. Since Ni is effectively one of the most common materials for SOFC anodes, this combination smoothly allows for ammonia feeding into such devices [46]. Indeed, Fournier et al. studied the functionality of Ni-, Pt- and Ag-based cermet anodes with ammonia, demonstrating that more than 90% of NH_3 was efficiently decomposed at 800 °C. Other elements such as Ag and Pt resulted almost half less efficient. With a YSZ electrolyte, a peak power density of 800 mW/cm^2 at 800 °C was demonstrated [48]. In the last years, more studies have been published regarding SOFC performances with ammonia, summarized in Table 2 as benchmarks. Currently, the highest maximum power density of 1190 mW cm^2 has been achieved by Meng et al. with ammonia in an oxygen ion conducting SOFC with 10 μm thick samarium-doped ceria (SDC) electrolyte, Ni-based anode and $Ba_{0.5}Sr_{0.5}Co_{0.8}Fe_{0.2}O_3$-based cathode at 650 °C [46,49,50].

Up to now, it has been demonstrated that ammonia-fed SOFCs operate through successive NH_3 decomposition (Eq. (2)) and H_2 electrochemical oxidation (Eq. (3)) [47,51,52].

$$2NH_3 \rightarrow N_2+3H_2 \qquad \text{Equation 2}$$

$$H2+ O2- \rightarrow H2O+2e- \qquad \text{Equation 3}$$

The catalytic decomposition of ammonia and electrochemical oxidation of hydrogen are the macro-processes which are effectively resulting from a set of elementary reaction mechanisms that involve adsorption and desorption, surface reactions and charge transfers. Different works suggested micro-kinetic models which confirm the two-step cracking and oxidation of the fuel with a multi-step adsorption-desorption mechanism of different gaseous species (NH_3, H_2, N_2). Fundamentally, adsorbed ammonia is step-by-step deprotonated on the surface-active sites with further proton and nitrogen recombination before associative desorption as H_2 and N_2 respectively. These models were consistent with experimental data, thus indicating reasonable insight into the reaction pathway [51,61]. Furthermore, the ammonia decomposition rate is sensibly dependent on the orientation of the catalyst facets as well as on the catalyst's microstructure [62,63].

Even if the electrochemical reaction is the same for both H_2- and NH_3-fueled SOFCs, the open circuit voltage (OCV) is still different for the two species. This phenomenon can be

Table 2 – State-of-the-art of SOFCs in terms of material components for electrodes and electrolyte, operating temperatures and achievable power densities.

Electrodes An-Cat	Electrolyte	Operating temperature [°C]	Power density [mW cm^2]	Reference
NiO/YSZ - Ag	YSZ	800	60	[48]
Ni/SDC - SSC/SDC	SDC	500–700	65–250	[53]
NiO - BSCF	SDC	550–650	167–1190	[50]
Ni/YSZ - YSZ/LSM	YSZ	750–850	299–526	[52]
NiO/SDC - SSC/SDC	SDC	650	467	[54]
Ni/YSZ - LSM	YSZ	700–900	38–88	[55]
Ni - SSC	SDC	600	168	[53]
NiO - BSCF	BZCY	450	135	[56]
Ni - BSCF	BCGO	600	147	[57]
Ni - LSC	BCGO	700	355	[58]
Pt	BCG	700	25	[59]
Ni - LSC	BCNO	700	315	[60]

ascribed to the lower partial pressure of hydrogen at the anode side when the cell is fed by ammonia. During ammonia decomposition, gaseous nitrogen is also produced, thus reducing the effect of the hydrogen partial pressure on the equilibrium potential [55]. Even if the OCV is a decreasing function of temperature, ohmic resistance and overpotentials of SOFCs decrease as the temperature is increased. This is due to many different reasons such as electrolyte conductivity, faster kinetics and faster diffusion. Hence, the optimal temperature during operation is a trade-off between reducing OCV and lowering overpotentials [51].

All this considered, ammonia seems to be a promising fuel for several applications ranging from automotive to stationary power production. The main concern linked to the utilization of ammonia regards the primary production. So far, the productive pathway of NH_3 is accompanied by considerable amounts of greenhouse gases emissions. The hydrogen source is mainly natural gas (72% of total production) which necessarily involves CO_2 emissions due to desulphurization, methane steam reforming and water gas shift reaction. Via this route, on average 3.45 equivalent tons of CO_2 are emitted per 1 ton of NH_3 produced [17,64].

For this reason, green ammonia production processes can be conceptualized and have raised scientific interest in the last decades. Solid state ammonia synthesis (SSAS) is one of the most promising techniques that seems to possess the potential for obtaining ammonia without emitting any significant GHG if the source of electrical power used for the electrochemical process comes from renewables [14,65–68].

This paper aims to investigate the performance of commercial oxygen-ion conducting solid oxide fuel cells (SOFCs) when fueled with hydrogen and ammonia. The state-of-the-art of ammonia as fuel for SOFCs is followed by the description and discussion of the experimental analysis. Particular attention is paid to the performance comparison of three cases where different flows feed the stack: hydrogen, a stoichiometric mixture of hydrogen and nitrogen (3:1 M ratio), and ammonia. The current-voltage characteristics have been evaluated for understanding the electrical behavior of the cell stack when different fuels are supplied. Additionally, the efficiency of the stack with hydrogen is compared to the one with ammonia, showing interesting results for this alternative fuel. Finally, considerations on the effective resistance of the stack are presented, with the scope of matching experimental data with analytical models that are used for modelling and simulating the cell behavior.

Experimental methodology

The tests on SOFC operation have been carried out at Fondazione Bruno Kessler facility with the test bench SSTB-01, provided by SOLIDpower S.p.A. The test bench is equipped with a small stack furnace that can reach 800 °C. The inlet and outlet gas temperatures are controlled via thermocouples in proximity of the stack. The thermocouple sensitivity is in the range of ±1.5 °C.

The gas interfaces are located at the rear of the bench allowing for inlet fluxes of ammonia, hydrogen, nitrogen, air and forming gas. The working pressure ranges between 3.0 and 5.0 bar while fluxes can vary from 0.1 to 10 NL/min for all the gases apart from air which can reach up to 50 NL/min. The inlet gas fluxes are mastered by *Voegtlin* mass flow controls with instrument uncertainty fixed at 1% of the maximum flow rates. In particular, the maximum flow rates for H_2, N_2, NH_3 and air were 5, 50, 5 and 50 NL/min, respectively.

The fuel cell stack provided by SOLIDpower S.p.A. is composed of 6 oxygen-ion conducting solid oxide fuel cells of 80 cm^2 of active area. The polarization curves have been recorded from 0 to 33 A and back to 0 when depolarizing, with specific customization of current gradients and steps. This current range was suggested by the supplier considering that the nominal power point should be obtained at 0.4 A/cm^2 (namely 32 A). Measurements have been performed with an *AGILENT N3300A* electronic load, whose uncertainties are 0.05% + 0.08 mV for voltage and 0.05% + 0.06 mA for current.

Working parameters and variables can be controlled through the TBCS software powered by *Labview*^{TM}. Different temperatures were set during various measurements to address changes in the stack functionality. Additionally, fluxes and fuel utilizations were specifically changed with the aim of investigating their effects on the SOFC operation. First, hydrogen was supplied to the stack for evaluating standard operating performances. Second, ammonia was injected to effectively address the functionality of the cells with such a fuel. Moreover, the effect of the endothermic reaction of ammonia cracking on the cell performances has been evaluated by performing tests with stoichiometric quantities of hydrogen and nitrogen and comparing them with an equivalent inlet of ammonia. The air flux has been fixed to 32 NL/min, corresponding to an oxygen utilization of 0.1 at the maximum current for all the tests.

Results

The first measurements on the fuel cells have been carried out with hydrogen as fuel with the intent of evaluating standard performances and obtaining reference results for the comparison with other fuels. In order to investigate the response of the stack with varying temperature, current-voltage curves have been measured at 670, 700, 730 and 760 °C. The same procedure carried out for hydrogen was then repeated for ammonia.

Fig. 2a, b shows the current-voltage characteristics for hydrogen and ammonia, respectively. The y-axis represents the voltage of the whole stack given as sum of the six single in-series cells' voltages. In this regard, Fig. 3 shows the polar representation of the voltages for each of the six cells composing the stack for the three different fuels that have been tested. The error values in the IV curves' measurements have been evaluated considering the experimental uncertainty on voltage and current (0.05% + 0.08 mV and 0.05% + 0.06 mA, respectively). The resulting errors have

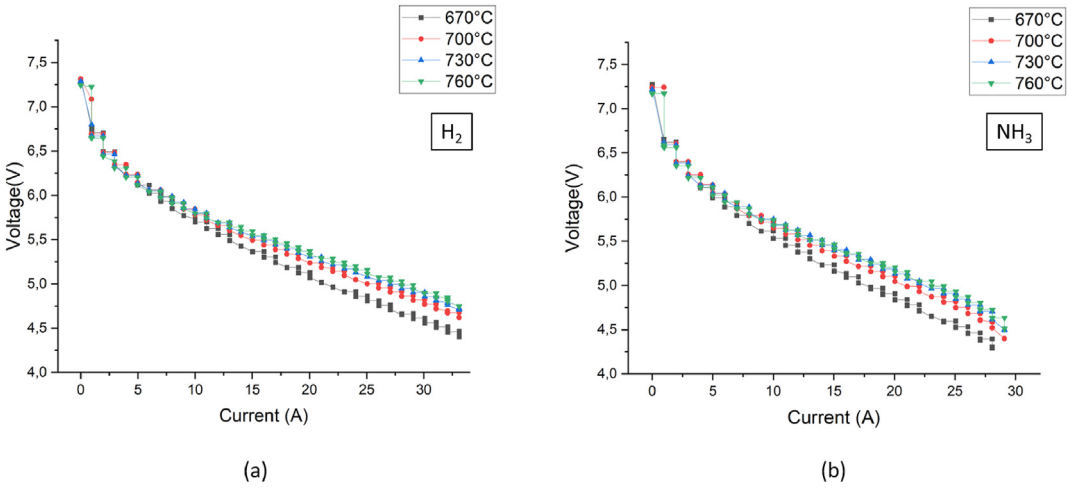

Fig. 2 – Current-voltage profiles at different temperatures for the tests with pure hydrogen (a) and pure ammonia (b). Voltage uncertainty: <0.002 V; current uncertainty: <0.01 A.

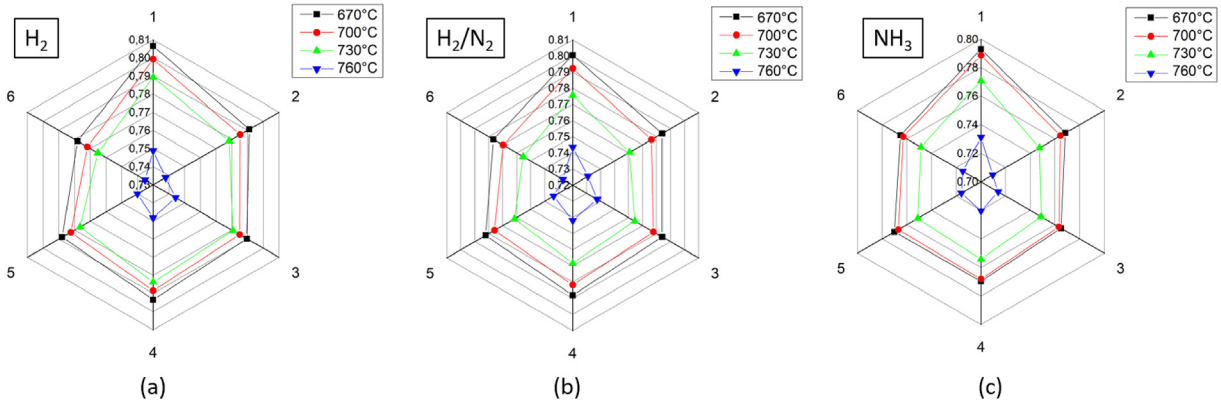

Fig. 3 – Polar representations of voltages for the six cells of the SOFC stack for the tests with hydrogen (a), stoichiometric mixture (b) and ammonia (c). Labels in the charts are to be read as 1 for the first cell at the bottom and 6 for the last cell at the top of the stack, respectively.

resulted to be several orders of magnitude smaller than the experimental measurements for both current and voltage (<0.01 A and <0.002 V, respectively). Therefore, for the sake of clarity, error bars are not shown in the IV profiles. As far as the error on power calculation is concerned, the uncertainty has been evaluated by considering a first-order Taylor series expansion for error propagation. Also in this case, the calculated error resulted significantly lower than the experimental values (<0.1 W) and therefore is not reported in Fig. 8. These small uncertainties in the experiments make the measurements reliable and suitable for comparison with previous works [22,26,30–37].

In order to understand the difference in operation when feeding the stack with hydrogen and ammonia, the feed flux has also been set as the stoichiometric composition in hydrogen and nitrogen coming from ammonia cracking. With hydrogen and nitrogen in 3:1 M ratio in NH_3, the feed mixture was composed of 1.726 NL/min in H_2 and 0.575 NL/min in N_2, corresponding to an ammonia flux of 1.150 NL/min as in the measurements with pure NH_3.

Fig. 4 shows the comparison between hydrogen, ammonia and the stoichiometric mixture at the different temperatures used in the experiments. The curves for hydrogen and for the mixture show higher voltages with respect to the ones relative to ammonia. To compare and validate the results with available data from literature, the testing conditions were chosen as similar as possible to the ones used in previous works. Aiming to reflect such conditions, when the stack was operated at 0.35 A/cm^2 (28 A), resulting cell voltages of 0.79 V for ammonia have been measured at 750 °C. Considering the values from other works at the same current density (0.35 A/cm^2) and equal or similar temperature range (700–800 °C) in the voltage range from 0.76 V to 0.85 V, our results seem to faithfully reflect the available literature data [22,26,30–37]. Deviations from the literature results can be attributed to the specific operating conditions such as inlet ammonia fluxes or fuel utilization.

Fig. 5 shows that at higher temperatures similar performances are obtained for ammonia than for hydrogen. Furthermore, in all the measurements with ammonia, the

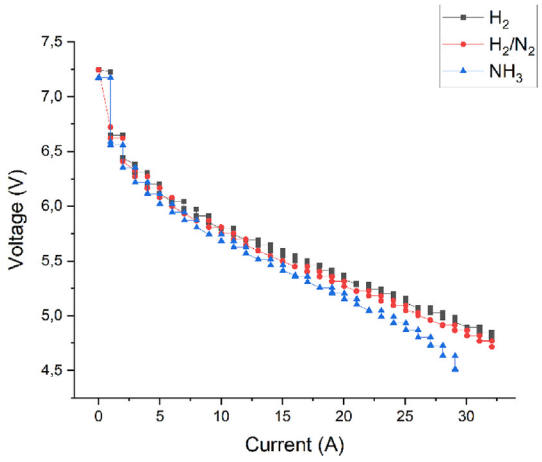

Fig. 4 – Comparison of the current-voltage profile for pure hydrogen (red dots), pure ammonia (black squares) and stoichiometric mixture of hydrogen and nitrogen (blue triangles) at 760 °C. Voltage uncertainty: <0.002 V; current uncertainty: <0.01 A. (For interpretation of the references to colour in this figure legend, the reader is referred to the Web version of this article.)

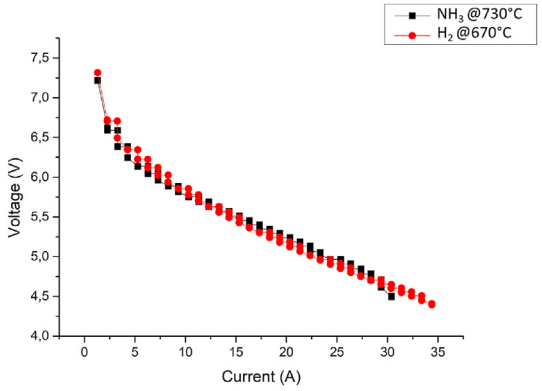

Fig. 5 – IV curves for ammonia feed at 730 °C (black squares) and pure hydrogen at 670 °C (red circles) showing a similar voltage drop. Voltage uncertainty: <0.002 V; current uncertainty:<0.01 A. (For interpretation of the references to colour in this figure legend, the reader is referred to the Web version of this article.)

polarization did not proceed smoothly for the whole polarization ramp until 33 A as it had been set.

When the current was raised to 28 A at 670 °C and to 29 A for the other temperatures, the voltage abruptly dropped down when injecting ammonia. Fig. 6 shows the final tail of IV curves for the three fuels used: H_2, NH_3 and the H_2/N_2 mixture. Linear trends are observed while using hydrogen and H_2/N_2 mixture as fuel while concentration losses are visible with ammonia above 27 A. Such evidence highlights as the voltage drop occurs for lower values of current when operating with ammonia. This caused the interruption of the polarization since a minimal threshold voltage of 0.68 V was fixed for each single cell (4.08 V for the stack). Below such voltage, the stack can be damaged since nickel in the anode can be subjected to

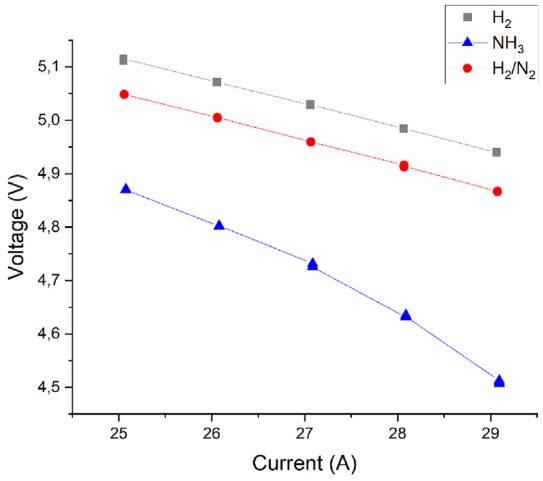

Fig. 6 – Voltage profiles at 760 °C for hydrogen (grey squares), stoichiometric mixture (red circles) and ammonia (blue triangles) at high current values. The ammonia voltage profile significantly departs from a linear trend, showing that concentration losses are earlier observable when ammonia is injected into the SOFC. Voltage uncertainty: <0.002 V; current uncertainty: <0.01 A. (For interpretation of the references to colour in this figure legend, the reader is referred to the Web version of this article.)

oxidation at high temperature, thus causing the transition to nickel oxide which is no longer active for the electrochemical oxidation of hydrogen [69–72].

Therefore, additional measurements with a larger ammonia flux have been performed for obtaining further insight regarding these performance limitations. Results are shown in Fig. 7.

Fig. 8 shows the electrical power obtained by the SOFC over the whole range of currents for all the tests. With hydrogen and the mixture, the extractable power results close to 170 W, larger than for ammonia (140 W).

Discussion

Performance comparison of SOFCs fueled with H_2, H_2/N_2 (3:1) and NH_3

For both fuels H_2 and NH_3, the voltage increases with the temperature when the cell is delivering current. This phenomenon is mainly attributed to the reduction in the internal resistance of the stack when increasing the temperature, which reflects the decrease in resistivity of the electrolyte in the cells and in overpotential losses at the interfaces.

Single cell performances are not identical, among others due to a thermal gradient in the furnace: bottom cells are at a lower temperature than the ones at the top. For this reason, the voltage increases for the top cells.

When comparing different fuels, the reason for observing a lower voltage profile with ammonia than with the other fuels can be ascribed to the reaction taking place in the furnace.

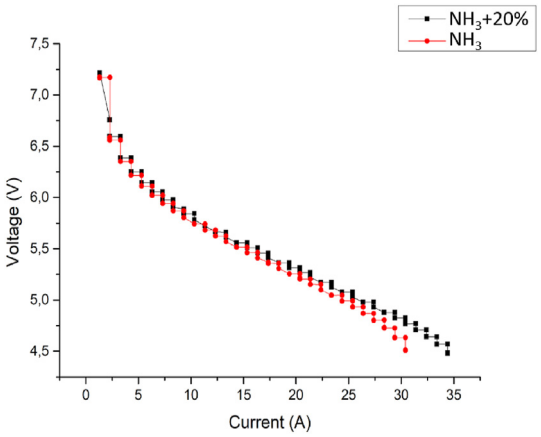

Fig. 7 – Comparison between polarization curves with different ammonia fluxes at 760 °C. Black-dotted curve for 20% increased ammonia flux does not abruptly fall at high currents because of concentration losses unlike the red-circled curve for lower feed flux. Voltage uncertainty: <0.002 V; current uncertainty: <0.01 A. (For interpretation of the references to colour in this figure legend, the reader is referred to the Web version of this article.)

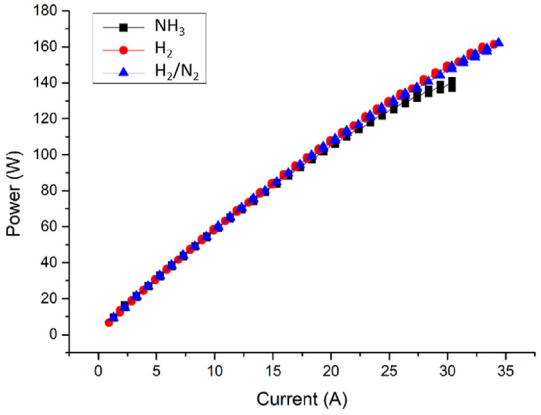

Fig. 8 – Comparison of the power-current profiles for pure hydrogen (red dots), pure ammonia (black squares) and stoichiometric mixture of hydrogen and nitrogen (blue triangles) at 760 °C. Power uncertainty: <0.1 W; current uncertainty: <0.01 A. (For interpretation of the references to colour in this figure legend, the reader is referred to the Web version of this article.)

When the cell is fed with ammonia, the ammonia thermally cracks before the electrochemical reaction of hydrogen occurs in the cell. Since ammonia cracking is an endothermic reaction, heat is absorbed from the stack, thus effectively decreasing the local temperature. Additionally, nitrogen reduces the hydrogen partial pressure. On the whole, the performances of the cell fed with hydrogen are achievable with ammonia at higher temperature. In this sense, Fig. 5 shows the comparison between the behavior for the test performed with ammonia at 730 °C (black line) and the one with hydrogen at 670 °C (red line), which are almost superimposed.

In order to indirectly get insight on the effect of ammonia cracking on the stack temperature, the temperature profiles of the inlet and outlet air fluxes have been analyzed for all the test temperatures and feed fluxes. A general trend could not be identified and the fluctuations around the average were smaller than ±1 °C, suggesting that the thermal contribution of ammonia dissociation did not affect the temperature of the furnace.

Furthermore, it can be noticed that the trend for NH_3 and H_2 is different at high current values. In Fig. 6 the portion of the voltage-current characteristic at 730 °C is magnified at values of current close to 28 A for the two feed gases. When considering hydrogen as inlet gas, the profile remains linear, meaning that concentration losses stay limited. Differently, the trend of IV curves for ammonia departs from a linear drop to lower voltage values. Such a behavior can be linked to increased concentration loss coming from a lack of reactants. A possible explanation might be that ammonia was not completely cracked, or not fast enough to feed the active sites at the anode at high currents. To this effect, a test with 20% more ammonia in the inlet flux has been carried out at 760 °C. Fig. 7 shows the complete polarization for the flux with increased ammonia content. By injecting 1.380 NL/min of NH_3, the polarization reached 33 A without reaching the lower safety threshold. This observation supports the fact that not enough fuel was reaching the cell in the test with lower flux and that the amount of available hydrogen is the only difference when a larger flux is used.

The difference in extractable power for H_2 and NH_3 firstly reflects the reduced range of current (0–29 A) over which the polarization occurred for ammonia with respect to pure hydrogen or the H_2/N_2 gas mixture (0–33 A). Secondly, as already observed, the voltage profile remains higher than that of ammonia over the whole range of current, thus resulting in higher values of power. The reduced fuel availability sensibly affected the voltage profile, thus leading to stack powers around 140 W for NH3 and almost 170 W for H2, at the maximum current points.

The efficiency (η) of the SOFC has been evaluated as the ratio of output and input power, according to Eq. (4):

$$\eta = \frac{I_{exp} V_{exp}}{\dot{M} LHV} \qquad \text{Equation 4}$$

where $\dot{M}$ is the mass flux of the inlet species and *LHV* is the corresponding lower heating value.

In such equation, the product of current and voltage representing the extractable power is evaluated for all the fuels (i.e. H_2, H_2/N_2 and NH_3) and temperatures at the same current density (0.35 A/cm^2) and same fuel utilization (0.68) in order to obtain a consistent comparison. The values of efficiencies for hydrogen and ammonia are reported in Table 3. The experimental uncertainty on the estimated efficiencies was evaluated based on a first-order Taylor expansion of the error propagation. Considering the previously mentioned values of uncertainty for current, voltage, and fluxes of H_2 and NH_3, the maximum uncertainty was estimated to be lower than 0.4% for hydrogen and 0.2% for ammonia.

The efficiencies increase as the temperature increases for both hydrogen and ammonia. This is coherent with the reduction of the electrolyte resistivity and with the voltage trends with increasing temperature. Electrochemical kinetics are faster at higher temperatures. This means that the

Table 3 – Efficiency values for hydrogen and ammonia at different operating temperatures. Efficiencies are calculated as ratio of output and input power, considering the LHV of the inlet fluxes and the electrical obtainable power as product of voltage and current at the same fuel utilization respectively. Values are calculated for a fixed current density (0.35 A/cm^2).

T [°C]	670		700		730		760	
FUEL	H_2	NH_3	H_2	NH_3	H_2	NH_3	H_2	NH_3
LHV [MJ/kg]	120,4	18,6	120,4	18,6	120,4	18,6	120,4	18,6
Vol flux [NL/s]	0,029	0019	0,029	0019	0,029	0019	0,029	0019
Mass flux [g/s]	0,003	0015	0,003	0015	0,003	0015	0,003	0015
P_{in} *[W]*	312,24	270,88	312,24	270,88	312,24	270,88	312,24	270,88
P_{out} *[W]*	130,8	121,2	136,4	126,9	138,9	129,6	139,9	130,1
η *[%]*	41,9	44,7	43,7	46,8	44,5	47,8	44,8	48,0

Table 4 – Comparison of conditions and efficiencies for ammonia fed SOFCs in our tests and in literature values.

T [°C]	Current density [A/cm^2]	η_{fuel}	η [%]	Ref
760	0.35	0.68	48	This work
750	0.35	0.7	52	[34]
750	0.35	0.8	56	[32]
700–800	0.35	1.0	63–70	[26]
763	/	0.55	30	[22]

equilibrium potential decreases with increasing temperature while the operating potential raises. Hence, the electrical efficiency becomes larger at higher temperatures.

Finally, it can be noticed that efficiencies obtained with ammonia are larger than those reached by feeding hydrogen. Values for ammonia as feeding gas are comparable to those found in literature as it can be seen in Table 4. Literature efficiencies might differ from the ones obtained here due to the different experimental parameters. The fuel utilization in this work was fixed at 0.68, consistently with the maximum value reached with ammonia flux. When considering similar fuel utilizations ($\eta_{fuel} = 0.70$), as used by *Barelli* et al., our efficiency value ($\eta = 48\%$) coherently reflects the value of 52% found by other researchers [34]. Considering different works and operational parameters, a certain degree of consistency can be observed. We expect that by raising the fuel utilization close to 1.0, efficiency would reach 60–70% as in *Dekker* et al. [26] A similar comparison can be made for the work of *Kishimoto* et al. [32], in which an efficiency of 56% has been observed for a fuel utilization of 0.8. In parallel, by lowering the fuel utilization for reaching similar values to those used by *Cinti* et al., the efficiency of the SOFC stack tested in the current study would reach 33%, which is very close to the 30% obtained by Cinti and co-workers [22].

Table 5 – Values of ASR for different fuels at different operating temperatures of the SOFC. The effective resistance has been evaluated at the voltage of 0.8 V by linearizing the voltage-current profile in the interval 0.7–0.9 V. ASR consistently decreases with temperature, showing larger values for ammonia than for hydrogen or hydrogen/nitrogen mixture.

T [°C]	ASR [Ω cm^2]		
	H_2	H_2/N_2	NH_3
670	0.688	0.704	0.840
700	0.624	0.648	0.760
730	0.592	0.616	0.728
760	0.576	0.592	0.696

Effective resistance of the stack

By considering the linear drop in the central range of currents, it has been possible to evaluate the effective resistance of the stack (ASR_{exp}) by simply dividing the voltage by the current as in Eq. (5):

$$ASR_{exp} = \frac{\Delta V}{\Delta i} \cdot A_{cell} \qquad \text{Equation 5}$$

where A_{cell} represents the cell area for dimensional consistency to the model. Values of ASR_{exp} obtained from experimental data are summarized in Table 5. The effective resistance is decreasing with increasing temperature, reflecting the reduction in electrolyte's resistivity. In addition, ASR for ammonia results slightly higher than that for hydrogen or mixture at all the operating temperatures, coherently to the more rapid voltage drop with increasing current.

The ASR_{exp} fundamentally describes all the resistances that the stack and the electrical connections oppose to the current flow. According to *Andersson* et al. [73], the effective area-specific resistance (ASR_{mod}) can be modelled in first approximation as an Arrhenius-type profile (Eq. (6)):

$$ASR_{mod} = ASR_0 exp\left[\frac{E_a}{R}\left(\frac{1}{T} - \frac{1}{T_0}\right)\right] \qquad \text{Equation 6}$$

where ASR_0 represents an area-specific resistance referred to a specific temperature T_0 taken as reference, E_a is an activation energy describing the whole set of barriers that the stack opposes to the current flow and R is the gas constant (8.314 J mol^{-1} K^{-1}).

This empirical correlation used in modeling can be rearranged to obtain a linear profile of the logarithm of the resistance (ln [ASR_{mod}]) against the inverse of the temperature (1/T). Fig. 9 shows a slight discrepancy between the supposed trend of the numerical model (red line) and the experimental data (black line). The modelling results tend to diverge from the experimental values at higher resistances as the temperature is decreased (larger values of 1/T). This means that the empirical model selected for describing the behavior of such variable does not perfectly fit for the temperature range of the tests. Nevertheless, it can be noticed that the general trend is still well represented by the model which clearly reflects the

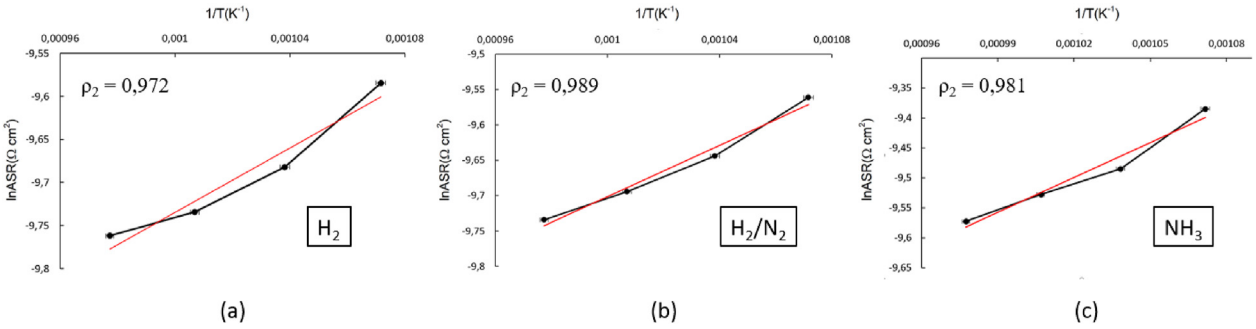

Fig. 9 – Trends of the area-specific resistance of the stack for hydrogen (a), stoichiometric mixture (b) and ammonia (b). Red lines represent linear fits of the experimental data (black dots) while values at left top correspond to the correlation index between the experimental values and the theoretical trend of the curve. Horizontal error bars account for temperature measurement uncertainty, while uncertainty in the ASR value from uncertainty propagation has resulted too small to be viewable (<1.8·10^{-5}). (For interpretation of the references to colour in this figure legend, the reader is referred to the Web version of this article.)

evidence that the effective resistance of the stack is reducing with temperature. This can be mainly ascribed to the reduction in resistivity of the electrolyte, thus favoring the flux of oxygen ions towards active sites.

Error estimation for both temperature and ASR was performed. In particular, the uncertainty in the temperature measurement was considered as the thermocouples' uncertainty (±1.5 °C). Consequently, the uncertainty of 1/T has been evaluated by uncertainty propagation and the horizontal error bars in Fig. 9 have been defined. For what concerns the ASR, the error was estimated considering a first-order Taylor expansion for uncertainty propagation and resulted to be < 1.8·10^{-5}. These values are too small to be reported on the graphs in Fig. 9 and, therefore, are not shown.

Even if the experimental trend does not strictly follow the empirical law expressed by the model, the model parameters have been evaluated by looking at the linear fitting ($E_{a,exp}$ and $ASR_{0,exp}$) according to Eq. (7):

$$lnASR = \frac{E_a}{R}\frac{1}{T} + lnASR_0 - \frac{E_a}{RT_0} \Rightarrow y = mx + q \qquad \text{Equation 7}$$

where $T_0 = 800$ °C has been assumed as reference temperature coherently to the modeling approach.

The activation energy can be obtained through the slope of the linear fit while the reference ASR_0 is related to the intercept with the y-axis. The reference area specific resistance $ASR_{0,exp}$ is compared to the literature value ($ASR_{0,mod}$). The results of the comparison are shown in Table 6. As it can be observed, the value of ARS_0 obtained from the modeling does not match with the experimental one. The reference value of the model is smaller than the one resulting from the experimental data. However, the ASR computed by the module are in the same order of magnitude as the experimental ones. This result leads to the conclusion that the model works fine as a first approximation for describing a general ASR trend. The reason for the observed mismatch is feasibly related to the fact that the model parameters (E_a, ASR_0, T_0) are strongly related to the investigated system (architectures, losses, etc …) and cannot be generalized. In particular, the choice of the values of ASR_0 and T_0 are not strictly valid for any systems at any operative temperature.

Table 6 – Comparison of modelling parameters for different feed fluxes when calculated from the modeling approach and when obtained directly from experimental data. ASR0 values do not perfectly match even if they remain in the same order of magnitude.

Feed	Slope	Intercept	$E_{a,exp}$ [kJ/mol]	$ASR_{0,mod}$ [$\Omega\ cm^2$]	$ASR_{0,exp}$ [$\Omega\ cm^2$]
H_2	2397.7	−12.096	19.934	2.9·10^{-5}*	5.2·10^{-5}
H_2/N_2	1135.1	−11.19	6618.34	2.9·10^{-5}*	3.9·10^{-5}
NH_3	2549.9	−12.07	21.199	2.9·10^{-5}*	6.1·10^{-5}

Conclusions

This paper presented a detailed performance comparison of oxygen-ion conducting SOFCs operating with hydrogen, ammonia, and a stoichiometric mixture of hydrogen and nitrogen (3:1 M ration). Differences, similarities, and correlations in the way these fuels allow for electrical power generation are pointed out in the framework of using ammonia as a promising energy vector by fueling SOFCs.

By polarizing the stack with currents ranging from 0 to 33 A at different temperatures, the evolution of the dynamic operation has been addressed. A small deviation to lower voltages has been observed for the stoichiometric mixture with respect to pure hydrogen, as a consequence of the lower hydrogen partial pressure in the feed. Voltages tend to decrease with temperature also for ammonia. However, the whole range of currents could not be investigated since concentration losses arose when reaching 28–29 A with ammonia. By testing the performance with an increased flux and observing polarizability up to 33 A, the hypothesis of incomplete or inefficient ammonia cracking seemed to be confirmed. As far as the electric power is concerned, higher values were obtained with hydrogen than with ammonia. On the whole, such evidence led to lower efficiencies for

hydrogen (close to 45%) than for ammonia (close to 48%) at the highest temperature (760 °C).

When investigating the ASR for different fuels, decreasing values from 0.7 to 0.6 Ωcm^2 with increasing temperature have been obtained for hydrogen and mixture, while values for ammonia range from 0.8 to 0.6 Ωcm^2. By comparing experimental results with numerical approaches used for modeling, a general accordance has been observed even if the trends are not perfectly matching, especially at the lowest temperatures.

These encouraging results evidence the potential for ammonia to become an alternative, efficient energy carrier. Further investigation on the performances of SOFCs with this fuel would be promising for understanding reaction mechanisms and limiting factors, with the aim of improving efficiencies and paving the way towards system integration as well as reversible operation for ammonia production via solid-state ammonia synthesis.

Declaration of competing interest

The authors declare that they have no known competing financial interests or personal relationships that could have appeared to influence the work reported in this paper.

Acknowledgements

The authors would like to acknowledge the Sustainable Energy (SE) center at Fondazione Bruno Kessler (FBK) for the support provided through their facilities and expertise. In addition, the authors would like to acknowledge the SOLIDpower group for supplying the cells' stack and experimental support. This research did not receive any specific grant from funding agencies in the public, commercial, or not-for-profit sectors.

REFERENCES

[1] International Renewable Energy Agency. Hydrogen from renewable power: technology outlook for the energy transition. https://www.irena.org/publications. [Accessed 18 November 2020].
[2] Ruf Y, et al. Fuel cells and hydrogen for green energy in European cities and regions. https://www.fch.europa.eu. [Accessed 18 November 2020].
[3] International Energy Agency (IEA). The Future of Hydrogen. Seizing today's opportunities. https://www.iea.org/reports/the-future-of-hydrogen. [Accessed 18 November 2020].
[4] European Commission. Hydrogen generation in Europe - overview of costs and key benefits. https://ec.europa.eu/energy/studies_main/final_studies/hydrogen-generation-europe-overview-costs-and-key-benefits_en. [Accessed 18 November 2020].
[5] Dincer Ibrahim, Acar Canan. Review and evaluation of hydrogen production methods for better sustainability. Int J Hydrogen Energy 2015;40(34):11094–111. https://doi.org/10.1016/j.ijhydene.2014.12.035.
[6] Kothari R, et al. Comparison of environmental and economic aspects of various hydrogen production methods. Renew Sustain Energy Rev 2008;12(2):553–63. https://doi.org/10.1016/j.rser.2006.07.012.
[7] Valera-Medina A, et al. Ammonia for power. Prog Energy Combust Sci 2018;69:63–102. https://doi.org/10.1016/j.pecs.2018.07.001.
[8] Ahmed Afif, et al. Ammonia-fed fuel cells: a comprehensive review. Renew Sustain Energy Rev 2016;60:822–35. https://doi.org/10.1016/j.rser.2016.01.120.
[9] Lan R, et al. Ammonia and related chemicals as potential indirect hydrogen storage materials. Int J Hydrogen Energy 2012;37(2):1482–94. https://doi.org/10.1016/j.ijhydene.2011.10.004.
[10] Aziz M, et al. Ammonia as effective hydrogen storage: a review on production, storage and utilization. Energies 2020;13(12):3062. https://doi.org/10.3390/en13123062.
[11] Valera-Medina A, et al. Review on ammonia as a potential fuel: from synthesis to economics. Energy Fuels 2021;35(9):6964–7029. https://doi.org/10.1021/acs.energyfuels.0c03685.
[12] Bicer Y, Farrukh K. Life cycle environmental impact comparison of solid oxide fuel cells fueled by natural gas, hydrogen, ammonia and methanol for combined heat and power generation. Int J Hydrogen Energy 2020;45(5):3670–85. https://doi.org/10.1016/j.ijhydene.2018.11.122.
[13] Wan Z, et al. Ammonia as an effective hydrogen carrier and a clean fuel for solid oxide fuel cells. Energy Convers Manag 2021;228:113729. https://doi.org/10.1016/j.enconman.2020.113729.
[14] Garagounis I, et al. Electrochemical synthesis of ammonia in solid electrolyte cells. Frontiers in Energy Research 2014;2:1. https://doi.org/10.3389/fenrg. 2014.00001.
[15] Rod TH, et al. Ammonia synthesis at low temperatures. J Chem Phys 2000;112(12):5343–7. https://doi.org/10.1063/1.481103.
[16] Weare W, et al. Catalytic reduction of dinitrogen to ammonia at a single molybdenum center. Proc Natl Acad Sci Unit States Am 2006;103(46):17099–106. https://doi.org/10.1073/pnas.0602778103.
[17] Giddey S, et al. Review of electrochemical ammonia production technologies and materials. Int J Hydrogen Energy 2013;38:14576–94. https://doi.org/10.1002/chin.201411236.
[18] Max appl. "Ammonia". *Ullmann's Encyclopedia of industrial chemistry*. American Cancer Society; 2006. https://doi.org/10.1002/14356007.a02_143.pub2.
[19] Scherer HW, et al. "Fertilizers 1". *Ullmann's Encyclopedia of industrial chemistry*. American Cancer Society; 2012. https://doi.org/10.1002/14356007.a10_323.pub3.
[20] Juangsa FB, et al. Production of ammonia as potential hydrogen carrier: review on thermochemical and electrochemical processes. Int J Hydrogen Energy 2021;46:14455–77. https://doi.org/10.1016/j.ijhydene.2021.01.214.
[21] Minutillo M, et al. Techno-economics of novel refueling stations based on ammonia-to-hydrogen route and SOFC technology. Int J Hydrogen Energy 2021;46(16):10059–71. https://doi.org/10.1016/j.ijhydene.2020.03.113.
[22] Cinti G, et al. Experimental analysis of SOFC fuelled by ammonia. Fuel Cell 2014;14(2):221–30. https://doi.org/10.1002/fuce.201300276.
[23] Cinti G, et al. SOFC operating with ammonia: stack test and system analysis. Int J Hydrogen Energy 2016;41(31):13583–90. https://doi.org/10.1016/j.ijhydene.2016.06.070.
[24] Vielstich W, et al. Handbook of fuel cells. Fundamentals, technology and applications. Wiley; 2010.
[25] Kalinci Y, Dincer I. Analysis and performance assessment of NH3 and H2 fed SOFC with proton-conducting electrolyte. Int J Hydrogen Energy 2018;43(11):5795–807. https://doi.org/10.1016/j.ijhydene. 2017.07.234.

[26] Dekker NJJ, Rietveld G. Highly efficient conversion of ammonia in electricity by solid oxide fuel cells. J Fuel Cell Sci Technol 2006;3:499–502. https://doi.org/10.1115/1.2349536.
[27] Wang S, Jiang SP. Prospects of fuel cell technologies. National Science Review 2017;4(2):163–6. https://doi.org/10.1093/nsr/nww099.
[28] Asmare M, İlbaş M. Direct ammonia fueled solid oxide fuel cells: a comprehensive review on challenges, opportunities and future outlooks. International Journal of Energy Technology 2020:70–91. https://doi.org/10.32438/ijet.203011.
[29] Hung YT, Shy SS. A pressurized ammonia-fed planar anode-supported solid oxide fuel cell at 1–5 atm and 750–850° C and its loaded short stability test. Int J Hydrogen Energy 2020;45(51):27597–610. https://doi.org/10.1016/j.ijhydene.2020.07.064.
[30] Wang Y, et al. Efficient and durable ammonia power generation by symmetric flat-tube solid oxide fuel cells. Appl Energy 2020;270:115185. https://doi.org/10.1016/j.apenergy.2020.115185.
[31] Jeerh G, et al. Recent progress in ammonia fuel cells and their potential applications. J Mater Chem 2020:727–52. https://doi.org/10.1039/D0TA08810B.
[32] Kishimoto M, et al. Development of 1 kW-class Ammonia-fueled solid oxide fuel cell stack. Fuel Cell 2020;20(1):80–8. https://doi.org/10.1002/fuce.201900131.
[33] Saadabadi SA, et al. Thermodynamic analysis of solid oxide fuel cell integrated system fuelled by ammonia from Struvite precipitation process. Fuel Cell 2020;20(2):143–57. https://doi.org/10.1002/fuce.201900143.
[34] Barelli L, et al. Operation of a solid oxide fuel cell based power system with ammonia as a fuel: experimental test and system design. Energies 2020;13(23):6173. https://doi.org/10.3390/en13236173.
[35] Stöckl B, et al. Ammonia as promising fuel for solid oxide fuel cells: experimental analysis and performance evaluation. ECS Transactions 2019;91(1):1601. https://iopscience.iop.org/article/10.1149/09101.1601ecst.
[36] Stöckl B, et al. Towards a wastewater energy recovery system: the utilization of humidified ammonia by a solid oxide fuel cell stack. J Power Sources 2020;450:227608. https://doi.org/10.1016/j.jpowsour.2019.227608.
[37] Hagen A, et al. Operation of solid oxide fuel cells with alternative hydrogen carriers. Int J Hydrogen Energy 2019;44(33):18382–92. https://doi.org/10.1016/j.ijhydene.2019.05.065.
[38] Al-Hamed K, Ibrahim D. A novel ammonia solid oxide fuel cell-based powering system with on-board hydrogen production for clean locomotives. Energy 2021;220:119771. https://doi.org/10.1016/j.energy.2021.119771.
[39] Wang Y, et al. Low–temperature ammonia decomposition catalysts for direct ammonia solid oxide fuel cells. J Electrochem Soc 2020;167(6):064501. https://doi.org/10.1149/1945-7111/ab7b5b.
[40] Alemu MA, Ilbas M. Direct ammonia powered solid oxide fuel cells: challenges, opportunities, and future outlooks. In: Journal of engineering and applied sciences technology; 2020. https://doi.org/10.47363/JEAST/2020-(2. SRC/JEAST-109.
[41] Ni M, et al. Ammonia-fed solid oxide fuel cells for power generation - a review. Int J Energy Res 2009;33(11):943–59. https://doi.org/10.1002/er.1588.
[42] Lan R, Shanwen T. Ammonia as a suitable fuel for fuel cells. Frontiers in energy research 2014;2:35. https://doi.org/10.3389/fenrg.2014.00035.
[43] Perna A, et al. Design and performance assessment of a combined heat, hydrogen and power (CHHP) system based on ammonia-fueled SOFC. Appl Energy 2018;231:1216–29. https://doi.org/10.1016/j.apenergy.2018.09.138.
[44] Wojcik A, et al. Ammonia as a fuel in solid oxide fuel cells. J Power Sources 2003;118(1):342–8. https://doi.org/10.1016/S0378-7753(03)00083-1.
[45] Farhad S, Hamdullahpur F. Conceptual design of a novel ammonia-fuelled portable solid oxide fuel cell system. J Power Sources 2010;195(10):3084–90. https://doi.org/10.1016/j.jpowsour.2009.11.115.
[46] Luo Y, et al. Coupling ammonia catalytic decomposition and electrochemical oxidation for solid oxide fuel cells: a model based on elementary reaction kinetics. J Power Sources 2019;423:125–36. https://doi.org/10.1016/j.jpowsour.2019.03.064.
[47] Ni M, et al. An improved electrochemical model for the NH3 fed proton conducting solid oxide fuel cells at intermediate temperatures. J Power Sources 2008;185(1):233–40. https://doi.org/10.1016/j.jpowsour.2008.07.023.
[48] Fournier GGM, et al. High performance direct ammonia solid oxide fuel cell. J Power Sources 2006;162(1):198–206. https://doi.org/10.1016/j.jpowsour.2006.06.047.
[49] Siddiqui O, Dincer I. A review and comparative assessment of direct ammonia fuel cells. Thermal Science and Engineering Progress 2018;5:568–78. https://doi.org/10.1016/j.tsep.2018.02.011.
[50] Meng G, et al. Comparative study on the performance of a SDC-based SOFC fueled by ammonia and hydrogen. J Power Sources 2007;173(1):189–93. https://doi.org/10.1016/j.jpowsour.2007.05.002.
[51] Ni M, et al. Thermodynamic analysis of ammonia fed solid oxide fuel cells: comparison between proton-conducting electrolyte and oxygen ion-conducting electrolyte. J Power Sources 2008;183(2):682–6. https://doi.org/10.1016/j.jpowsour.2008.05.022.
[52] Ma Q, et al. A high-performance ammonia-fueled SOFC based on a YSZ thin-film electrolyte. J Power Sources 2007;164(1):86–9. https://doi.org/10.1016/j.jpowsour.2006.09.093.
[53] Ma Q, et al. Direct utilization of ammonia in intermediate-temperature solid oxide fuel cells. Electrochem Commun 2006;8(11):1791–5. https://doi.org/10.1016/j.elecom.2006.08.012.
[54] Liu M, et al. Direct liquid methanol-fueled solid oxide fuel cell. J Power Sources 2008;185(1):188–92. https://doi.org/10.1016/j.jpowsour.2008. 06.076.
[55] Fuerte A, et al. Ammonia as efficient fuel for SOFC. J Power Sources 2009;192(1):170–4. https://doi.org/10.1016/j.jpowsour.2008.11.037.
[56] Lin Y, et al. Proton-conducting fuel cells operating on hydrogen, ammonia and hydrazine at intermediate temperatures. Int J Hydrogen Energy 2010;35(7):2637–42. https://doi.org/10.1016/j.ijhydene.2009.04.019.
[57] Zhang L, Yang W. Direct ammonia solid oxide fuel cell based on thin proton conducting electrolyte. J Power Sources 2008;179(1):92–5. https://doi.org/10.1016/j.jpowsour.2007.12.061.
[58] Ranran P, et al. Electrochemical properties of intermediate-temperature SOFCs based on proton conducting Sm doped BaCeO3 electrolyte thin film. Solid State Ionics 2006;177(3):389–93. https://doi.org/10.1016/j.ssi.2005.11.020.
[59] Maffei N, et al. A direct ammonia fuel cell using barium cerate proton conducting electrolyte doped with gadolinium and praseodymium. Fuel Cell 2007;7(4):323–8. https://doi.org/10.1002/fuce.200600038.
[60] Li Z, et al. Preparation of double doped BaCeO3 and its application in the synthesis of ammonia at atmospheric pressure. Sci Technol Adv Mater 2007;8(7):566–70. https://doi.org/10.1016/j.stam.2007.08.009.
[61] Appari S, et al. Micro-kinetic modeling of NH3 decomposition on Ni and its appli- cation to solid oxide fuel cells. Chem Eng

Sci 2011;66(21):5184–91. https://doi.org/10.1016/j.ces.2011.07.007.
[62] Kishimoto M, et al. Formulation of ammonia decomposition rate in Ni-YSZ anode of solid oxide fuel cells. Int J Hydrogen Energy 2017;42(4):2370–80. https://doi.org/10.1016/j.ijhydene.2016.11.183.
[63] Jiao F, Xu B. Electrochemical ammonia synthesis and ammonia fuel cells. Adv Mater 2019;31(31):1805173. https://doi.org/10.1002/adma.201805173.
[64] Yapicioglu A, Dincer I. A review on clean ammonia as a potential fuel for power generators. Renew Sustain Energy Rev 2019;103:96–108. https://doi.org/10.1016/j.rser.2018.12.023.
[65] Kyriakou V, et al. Progress in the electrochemical synthesis of ammonia. Catal Today 2017;286:2–13. https://doi.org/10.1016/j.cattod.2016.06.014.
[66] Amar IA, et al. Solid-state electrochemical synthesis of ammonia: a review. J Solid State Electrochem 2011;15(9):1845. https://doi.org/10.1007/s10008-011-1376-x.
[67] Liu H. Ammonia synthesis catalyst 100 years: practice, enlightenment and chal- lenge. Chin J Catal 2014;35(10):1619–40. https://doi.org/10.1016/S1872-2067(14)60118-2.
[68] Marnellos G, Stoukides M. Ammonia synthesis at atmospheric pressure. Science 1998;282(5386):98–100. https://doi.org/10.1126/science.282.5386.98.
[69] Neidhardt J, et al. Kinetic modeling of nickel oxidation in SOFC anodes. ECS Transactions 2011;35(1):1621. https://doi.org/10.1149/1.3570148.
[70] Sarantaridis D, Atkinson A. Redox cycling of Ni-based solid oxide fuel cell anodes: a review. Fuel Cell 2007;7(3):246–58. https://doi.org/10.1002/fuce.200600028.
[71] Tikekar NM, et al. Reduction and reoxidation kinetics of nickel-based SOFC anodes. J Electrochem Soc 2006;153:4. https://doi.org/10.1149/1.2167949. A654.
[72] De Angelis S, et al. Ex-situ tracking solid oxide cell electrode microstructural evolution in a redox cycle by high resolution ptychographic nanotomography. J Power Sources 2017;360:520–7. https://doi.org/10.1016/j.jpowsour.2017.06.035.
[73] Andersson D, et al. Dynamic modeling of a solid oxide fuel cell system in Modelica. Proceedings of the 8th international modelica conference, No. 63. Linköping University Electronic Press; 2011. https://doi.org/10.1115/FuelCell2010-33053. March 20th-22nd; Technical Univeristy; Dresden; Germany.